Available online at www.sciencedirect.com
ScienceDirect
International Journal of Machine Tools & Manufacture 47 (2007) 2282–2289
INTERNATIONAL JOURNAL OF MACHINE TOOLS & MANUFACTURE DESIGN, RESEARCH AND APPLICATION
www.elsevier.com/locate/ijmactool

Polishing of polycrystalline diamond by the technique of dynamic friction, part 3: Mechanism exploration through debris analysis

Y. Chen, L.C. Zhang*, J.A. Arsecularatne, I. Zarudi

School of Aerospace, Mechanical and Mechatronic Engineering, The University of Sydney, NSW 2006, Australia

Received 11 December 2006; received in revised form 5 June 2007; accepted 6 June 2007
Available online 10 July 2007

Abstract

This paper investigates the mechanisms of material removal in dynamic friction polishing of polycrystalline diamond composites through the analysis of polishing-produced debris. The specimens used were PCD compacts composed of diamond and silicon carbide. In order to uncover the debris' structure, high-resolution transmission electron microscopy (HRTEM), electron diffraction and electron energy loss spectroscopy (EELS) were used. Additionally, the density and the sp^2 to sp^3 ratio in the hybridized carbon materials of the debris were estimated from the EELS spectra. It was found that the debris were mainly of amorphous structure and consisted of different forms of carbon, silicon oxide/carbide, iron oxides, etc. The results show that during polishing, the diamond has transformed to non-diamond carbon, and silicon carbide to amorphous silicon carbide/oxide.

Keywords: Dynamic friction polishing; Polycrystalline diamond; Material removal mechanism; Phase change; Debris; Silicon carbide

1. Introduction

As discussed in part 1 of this series research [1], the dynamic friction polishing (DFP) technique utilizes the thermo-chemical reaction induced by the dynamic friction between a diamond specimen and a metal disk rotating at a high peripheral speed to enable an efficient abrasive-free polishing of single and polycrystalline diamond [2–5]. A model has been developed to predict the temperature rise of the PCD surface during polishing [1]. However, the material removal mechanisms are still to be understood.

Iwai et al. [3] and Suzuki et al. [4] investigated the dynamic friction polishing process based on the polishing efficiency in various atmospheres, and carried out X-ray diffraction analyses of the polishing debris and the surface of metal disk tool. They suggested that rapid diffusion of carbon from the diamond to the disk and then evaporation of carbon by oxidization were the mechanisms. They ruled out the possibility of carbonization of diamond because they did not find graphite in polishing debris and on the metal disk surface after polishing.

In part 2 of this series research [6], using scanning electron microscopy (SEM), energy dispersive X-ray (EDX), X-ray diffraction and Raman spectroscopy, Chen et al. [6] found non-diamond carbons (both sp^2 and sp^3) on the polished specimen surfaces, but only sp^3 carbon in polishing-produced debris. There was no indication of presence of graphite from the debris, although low intensity graphite band (Raman peak at 1588 cm^{-1}) was detected in polished specimens. They suggested that the surface graphite, which converted from diamond, was likely to oxidize in the oxygen environment and escape as CO/CO_2 gas although some of the converted graphite was found on the polished PCD specimens before surface cleaning. It is possible that the converted graphite remains inside debris but could not be detected by Raman spectroscopy which often lacks the spatial resolution for phase identification in nanocrystalline structures.

The aim of the present work is to investigate the polishing-produced debris with high-resolution transmission electron microscopy (HRTEM) and electron diffraction and electron energy loss spectroscopy (EELS) to reveal

*Corresponding author.
E-mail address: zhang@aeromech.usyd.edu.au (L.C. Zhang).

0890-6955/$ - see front matter © 2007 Elsevier Ltd. All rights reserved.
doi:10.1016/j.ijmachtools.2007.06.004

the electronic structure of the debris material and different phases of carbon, respectively. Because the characteristic peak reveals the presence of π electrons, an estimate of the percentage of sp^2-hybridized carbon in the debris can also be made. In this way, a detailed analysis of polishing-produced debris can be obtained including the microstructure, chemical composition and bonding information. Hopefully, this will facilitate a deeper understanding of the dynamic friction polishing mechanisms, and throw new light on whether chemical/phase transformations occur during polishing.

2. Experiment

The PCD specimens used were thermally stable diamond compacts, containing 70–75% diamond particles of 25 μm in grain size (the rest are SiC and Si). The diameter and thickness of a typical specimen were 12.7 and 4 mm, respectively. The thermal conductivity of the specimen material was 300 W/mK.

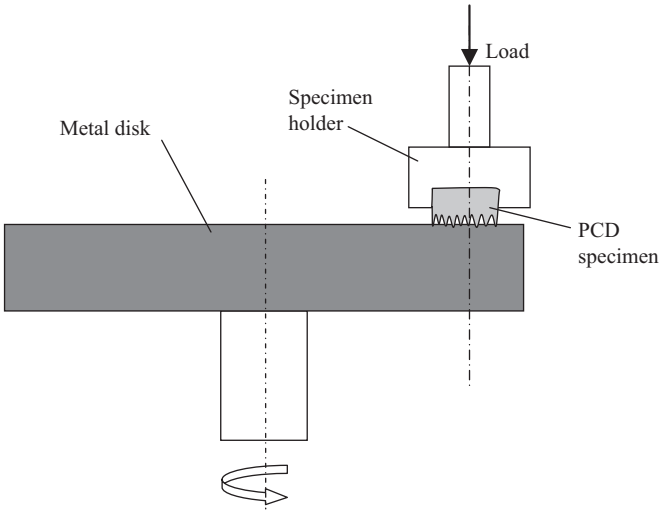

Fig. 1. Schematic illustration of dynamic friction polishing.

The polishing experiments were conducted on a polishing machine manufactured in-house, as illustrated in Fig. 1. Polishing was conducted by pressing a PCD specimen on to a rotating catalytic metal disk in dry atmosphere. The polishing parameters were: average sliding speed in the range of 15–25 m/s, pressure from 3 to 7 MPa, and polishing time from 1 to 5 min. At the end of a test, the polishing debris were collected from around a PCD surface.

The transmission electron microscopy (TEM) samples of polishing debris were prepared as follows. The debris were mixed with ethanol and crunched to very fine particles with a pestle and mortar. This mixture was transferred to a small container and further broken down in an ultrasonic bath for 5 min. The solution was allowed to settle for 5 min and then the top section of the suspension was collected. With a TEM grid sitting on filter paper, around 10–15 drops were applied to the TEM grid, allowing time between each drop for the excess solution to be absorbed by the filter paper. In sample preparation, the temperature throughout a specimen was kept below 40 °C to ensure that no micro-structural changes took place.

The conventional TEM studies were carried out using a Philips CM12, operating at 120 kV. The HRTEM investigations were performed on a JEOL JEM-3000F, operating at 300 kV. The samples were also studied in scanning transmission electron microscope (STEM) VG HB601. Meanwhile, EDX was used to investigate the chemical compositions of the interested subsurface layers. On the other hand, to evaluate the atomic bonding in interested spot, EELS with 1 μm probe diameter was employed.

Because of the relatively large amount of debris particles on the copper grid with a supporting holey carbon film, it was difficult to find areas where the structure of the material would be revealed. To overcome the problem, the attached EDX (in HRTEM or STEM) was used to exclude the metal rich areas and detect the elements of carbon and silicon, which come from the polishing PCD specimen. Further, EELS and HRTEM analyses were mainly

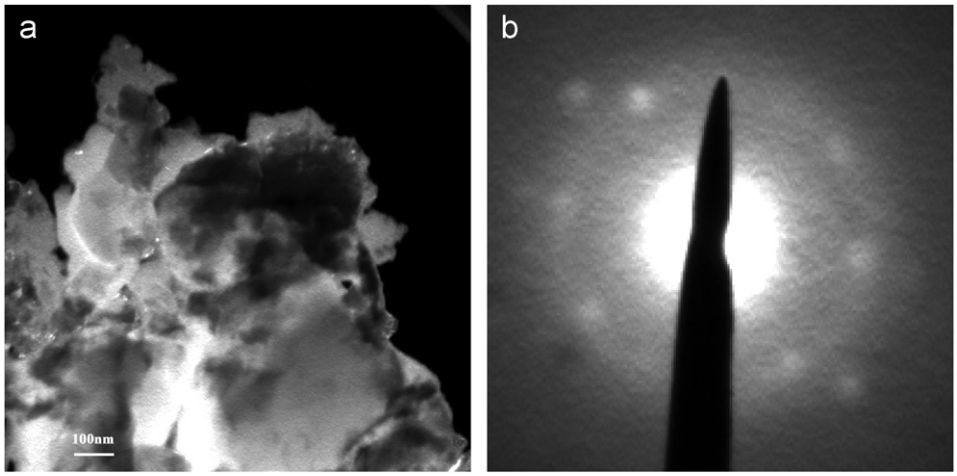

Fig. 2. TEM analysis of polishing debris: (a) TEM image and (b) diffraction pattern.

performed on areas that contained carbon and/or silicon. In order to prevent contamination by the holey carbon film, the EELS spectra of carbon were only taken from the particles on the hole of the carbon support film.

3. Results and discussion

3.1. Microstructure and composition of debris

Fig. 2 shows a typical TEM image of a piece of debris and its electron diffraction pattern, which indicates that the polishing debris consisted of SiC, Fe_3O_4 and graphite. These halos (faint ring) patterns also indicate that the polishing debris were amorphous, consistent with the very weak XRD peak reported in Ref. [6]. Through conventional TEM, it was found that almost all the polishing debris were amorphous, and that only little part of the debris showed the F_2O_3 crystal structure.

According to the EDX analysis, the debris contained carbon, oxygen, silicon, iron, chromium and nickel, which were similar to the EDX analysis in SEM reported by Ref. [6]. Some spots/areas consisted only a few of the above elements. Since the elements iron, chromium and nickel came from the metal disk, areas containing only these elements and oxygen were not considered for further analysis.

Fig. 3 shows three typical high-loss spectra of carbon from different pieces of polishing debris. To understand the structure of the material, the four high-loss spectra for graphite, diamond, amorphous carbon and diamond-like carbon (DLC) are shown in Fig. 4 [7–9,12] for reference. It is clear that diamond has a single loss feature with an onset at about 290 eV owing to its σ* electronic states while graphite has an additional absorption starting at around 285 eV due to its lower lying antibonding π* states [10]. Amorphous or disordered carbon has a peak at about 285 eV, similar to graphite but with different intensity. By comparison, the high-loss spectra of carbon in polishing debris correspond to DLC (Fig. 3(a)), graphite (Fig. 3(b)) and amorphous carbon (Fig. 3(c)), but not diamond. It can be seen that transformation of diamond to different forms of non-diamond carbon took place during dynamic friction polishing.

Though the majority of the debris material appeared to be amorphous, high-resolution images of these debris reveal the presence of crystallities in an "amorphous" matrix, because some fringe groups are present in the matrix. Fig. 5 shows three typical HRTEM images of the polishing debris. The fringe spacing in Fig. 5(a) is 3.55 Å, implying that ordered hexagonal Fe_2O_3 regions may exist. Fig. 5(b) shows an HRTEM image of the area where graphite EELS spectrum was collected (Fig. 3(b)), the interlayer distance between the small layers visible in the material was measured to be 3.36 Å, which corresponds to the interlayer distance in graphite. The material seems to be built up of a number of areas, where a number of graphite planes appear to be stacked either in an approximately straight and parallel or concentric or entirely disordered fashion. In Fig. 5(c), which corresponds to the amorphous carbon EELS spectrum (Fig. 3(c)), the material seems to contain very small nanometer-sized graphitic structures (interlayer distance of 3.35 Å) and may best be described as disordered graphite. In addition, small crystalline areas with lattice spacing of 3.35 Å are visible within the amorphous material. However, no fringe group was observed in the areas where the EELS spectra of DLC (Fig. 3(a)) were collected. It might exist in amorphous forms in polishing debris, as indicated by a broad band in Raman spectra [6]. No diamond was observed in the polishing debris.

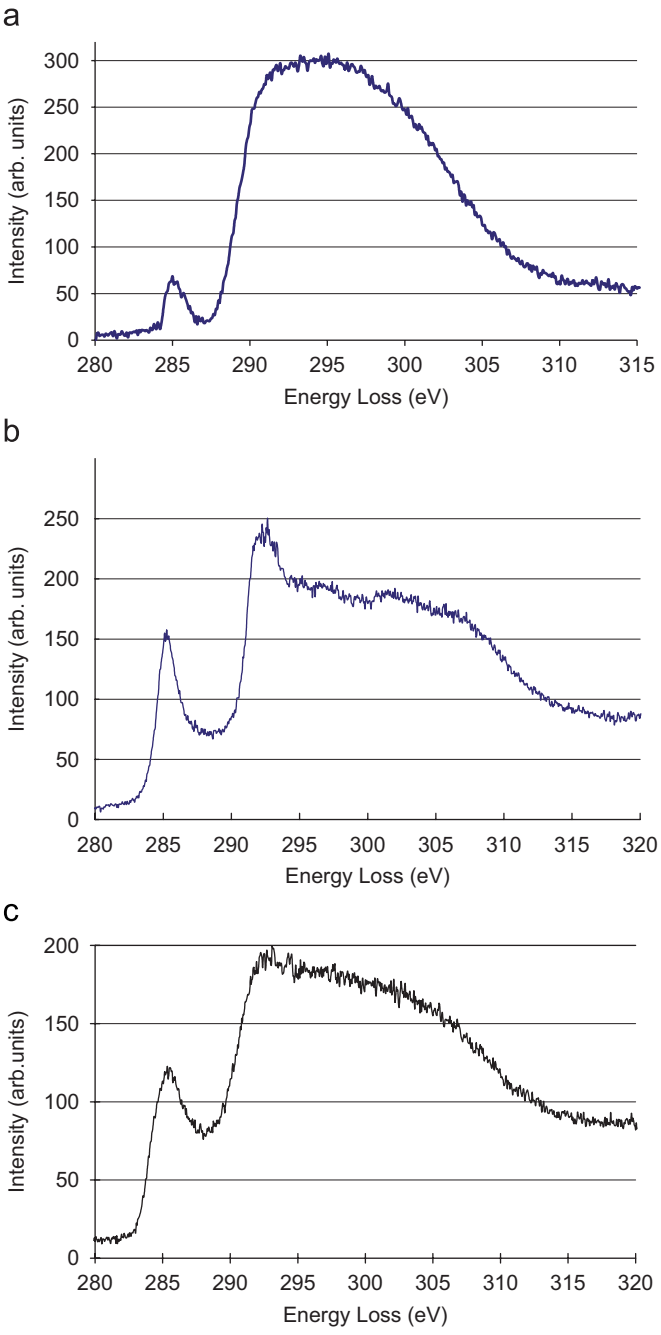

Fig. 3. High-loss carbon spectra of polishing debris: (a) DLC, (b) graphite and (c) amorphous carbon.

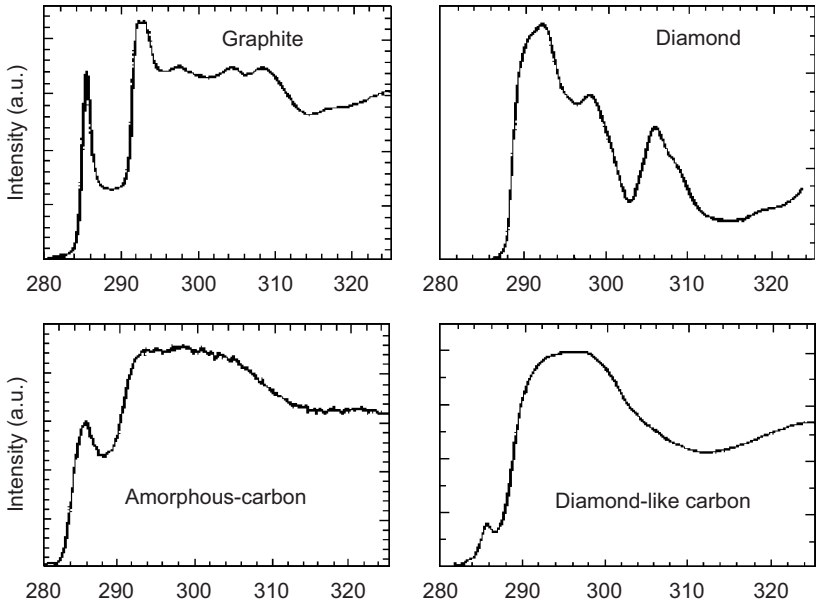

Fig. 4. High-loss spectra of carbon [12].

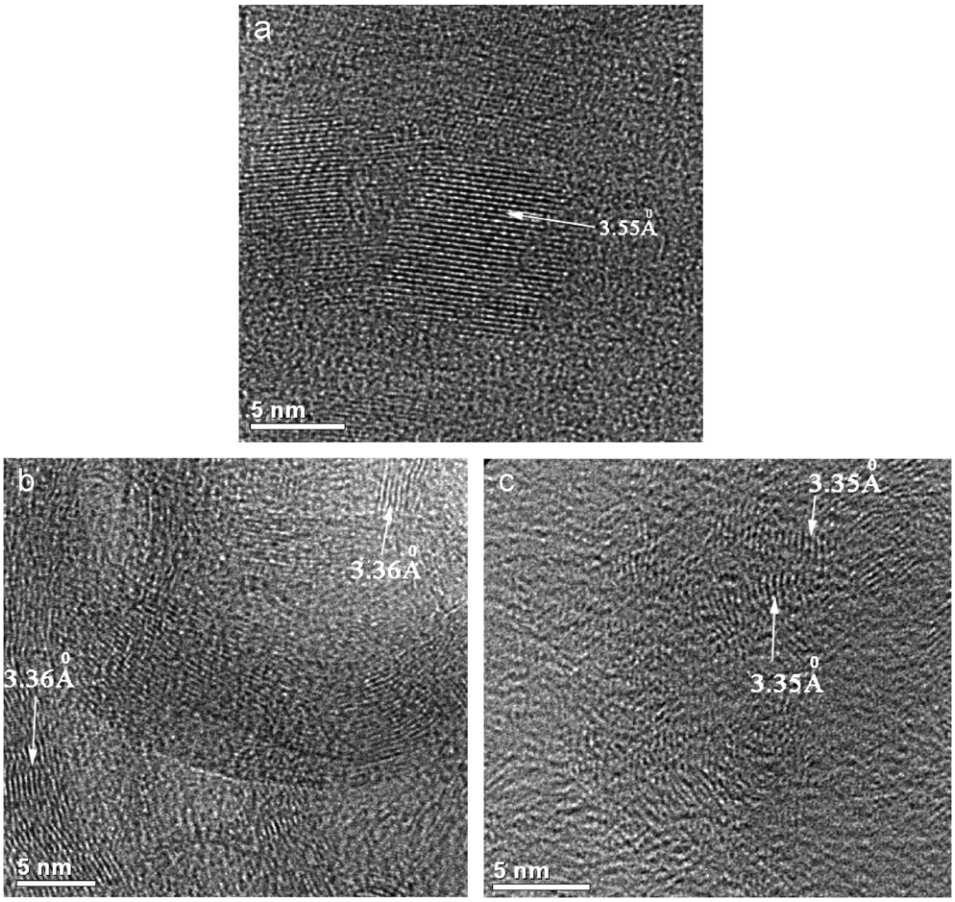

Fig. 5. Typical HRTEM of polishing debris: (a) Iron oxide, (b) graphite and (c) amorphous carbon.

3.2. Density of the transformed materials

Typical low-loss EELS spectra, corresponding to high-loss spectra of DLC (Fig. 3(a)), graphite (Fig. 3(b)) and amorphous carbon (Fig. 3(c)) are shown in Fig. 6. The peak of the bulk plasmon energy lies between 22.3 and 26.5 eV for the different debris regions. For comparision, the plasmon peak of diamond is at 33 eV [8]. From

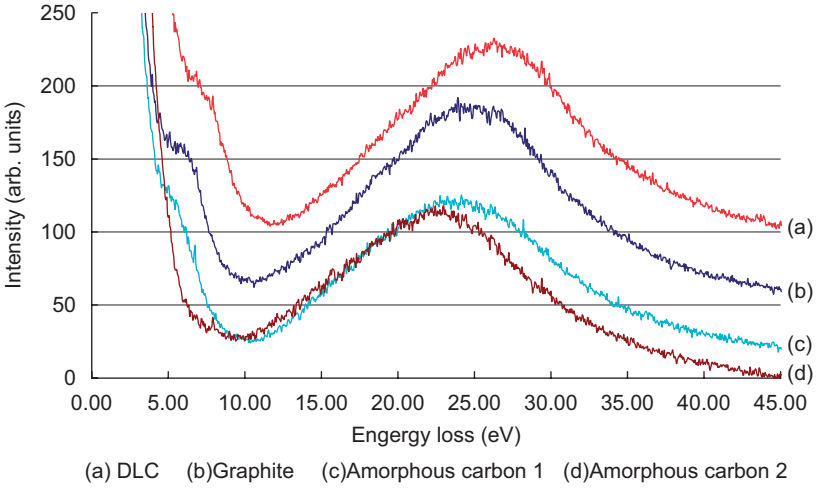

Fig. 6. Low-loss carbon spectra of polishing debris.

the low-loss spectrum, the density of the debris material can be estimated. The bulk plasmon energy corresponds to the high peak in the graph. According to the free electron theory, the energy E_p of the bulk plasmon is given by [11]

$$E_p = \sqrt{\frac{n_c \hbar^2 e^2}{4\pi^2 m \varepsilon_0}},$$

where n_c is the number of valence electrons per unit volume, $\hbar$ Planck's constant, ε_0 the permittivity of free space, m and e are the effective electron mass and charge. Assuming four valence electrons per atom, the density of the debris can be calculated from the plasmon energy. The effective mass density ρ is proportional to the charge density n_c [12]

$$\rho = \frac{M n_c}{n_v N_A} = \frac{3 n_c}{N_A},$$

where N_A is the Avogadro's number, M the atomic weight ($=12$ for carbon) and n_v is the mean number of valence electrons per atom ($=4$ for carbon, assumed). The densities of the various forms of carbon in the debris calculated this way are shown in Table 1. It can be seen that the densities vary in the range of 1.8–2.5 g/cm^3.

It is known that the densities of diamond, graphite and amorphous carbon are 3.5, 2.3 and 1.8 g/cm^3, respectively [13]. Although the free electron theory is only an approximation, the marked change in the densities clearly shows that conversion of diamond to less dense forms of carbon has occurred during polishing, confirming the observation from the high-loss spectra. The different densities may be a result of the carbon bonding in different sp^2 to sp^3 ratios and the different ways of clustering during polishing [14].

3.3. Atomic bonding

It is known that different forms of carbon have differing types of bonding. Perfect diamond has 100% sp^3 bonding, graphite has 100% sp^2 bonding, while DLC and amorphous carbon can have variable sp^2/sp^3 bonding ratios [13]. Therefore, the analysis of the sp^2/sp^3 carbon ratio of the polishing debris can provide the bonding information, and further confirm whether the transformation of diamond to non-diamond carbon has occurred, which would give an indication of the mechanisms involved in the polishing process.

Table 1
Densities of the carbon materials in debris estimated from the plasmon energies in Fig. 6

Debris	Plasmon energy (eV)	Density (g/cm^3)
(a) DLC	26.5	2.5
(b) Graphite	25.0	2.2
(c) Amorphous carbon 1	24.0	2.0
(d) Amorphous carbon 2	22.3	1.8

From the high-loss (carbon K edges) spectra it is possible to calculate the sp^2 to sp^3 ratio of the carbon material in the debris. The amount of sp^2 bonding can be deduced from the area of the 1 s–π* transition in the carbon high-loss spectrum [8,9]. Excitations of 1 s electrons in the ground state to π* states result in characteristic sharp π-peaks observed in the regions around 285 eV ($282 < \Delta E < 286$ eV). Excitations to the σ* states occur at higher energy levels. According to Schmid [8], the fraction of the sp^2 bonded atoms in the debris can be estimated by considering the integrated intensity of π-peak in unknown forms of carbon normalized by that of 100% sp^2 bonded graphite. In other words, the fraction f of sp^2 bonded atoms in the debris can be determined by [8]

$$f = \left(\frac{\bar{I}_d}{\bar{I}_g}\right)_\pi,$$

where $\bar{I}_d = (I_{d\pi})/(I_d(\Delta E))$ and $\bar{I}_g = (I_{g\pi})/(I_g(\Delta E))$ in which $I_{d\pi}$ is integrated intensity of the π-peak in the debris, $I_{g\pi}$ the integrated intensity of the π-peak in graphitized

carbon which represents 100% sp^2 bonding, and $I_d(\Delta E)$ and $I_g(\Delta E)$ are the integrated intensities of I_d and I_g, respectively, over sufficiently large energy widows ΔE (e.g. 280–320 eV). In the above notations, subscripts "d" and "g" indicate "debris" and "graphite", respectively.

By using the above method and the high-loss EELS spectra of carbon, the percentages of sp^2 bonding in the debris were estimated to be approximately 30% in DLC (Fig. 3(a)), 90% in graphite (Fig. 3(b)), and 85% in amorphous carbon (Fig. 3(b)). These results further confirm the structures of different phases of non-diamond carbon. This analysis and the TEM microscopy and EELS spectroscopy discussed earlier clearly show that the debris mainly consist of non-diamond amorphous carbon.

3.4. Chemical reaction of SiC during polishing

Further investigations were performed in the silicon rich area, as detected by EDX. Fig. 7 shows the EELS spectrum of silicon and the HRTEM of the silicon rich area. By comparing these results with those in the literature [15,16], the spectrum (Fig. 7(a)) can be assigned to silicon oxide (SiO_2). According to HRTEM of the silicon rich area (Fig. 7(b)), it seems to contain two regions: (1) the left middle region, where the interlayer distance was recognized to be 4.83 Å, corresponding to the interlayer distance in iron oxide; and (2) the right bottom region which mainly contains amorphous phase with only small crystalline area of which a few lines match lattice spacing of 1.46 Å of SiO_2. In other areas, there was no clear lattice spacing of SiO_2 in the collected EELS of silicon oxide visible, possibly due to its amorphous structure. It seems that the amorphous SiO_2 would mix with iron oxide in forming polishing debris. Moreover, while the diamond grains in the PCD polishing interface were transformed to non-diamond carbon, the remaining SiC skeleton would be consequently exposed to oxygen at elevated temperature, and the following chemical reaction was likely to occur:

$$SiC + 2O_2 \rightarrow SiO_2 + CO_2$$

The reaction product SiO_2 was found in amorphous phase and was much softer than SiC. It was removed mechanically by the high-speed rotating disk. The remaining skeleton SiC then became weaker and was also removed.

3.5. Polishing mechanism

From a theoretical model developed to predict the temperature rise in dynamic friction polishing [1,6], the PCD-metal interface temperature was estimated to be above 1270 K. The high temperature would stimulate the reactions between the polishing metal disk and diamond at the interface. While PCD was being polished, on the contact asperities of the PCD surface, the interface temperature had risen above the critical point of the fast transformation of diamond due to the frictional heating. The contacting catalyst metals would accelerate the transformation of diamond to non-diamond carbon. From the Raman analysis, these non-diamond carbons were detected on the polished metal adhered surface and in the polishing debris, indicating that transformation had occurred during polishing [6]. The results presented above have further confirmed the transformation of diamond to non-diamond carbons (sp^2 and sp^3 bonding), which can be considered as the basic process of the dynamic friction polishing. Meanwhile, another component of PCD, SiC also chemically reacted and transformed to amorphous silicon oxide/carbide. After the transformation, the surfaces of the contact asperities became softer and were removed mechanically with some of the adhered metal/oxide due to the relative motion between the disk and PCD surface. After the transformed layer and adhered film were removed, new asperities would contact with the catalyst metal. The repetition of this process ultimately results in polishing the PCD surface.

Fig. 8 summarizes the material removal mechanisms and the associated chemical reactions in dynamic friction polishing process.

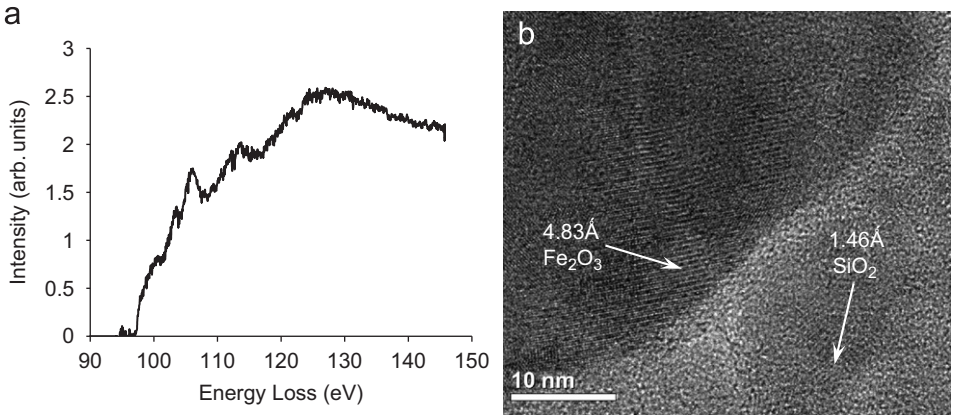

Fig. 7. EELS spectrum and HRTEM image of silicon rich area: (a) EELS spectrum and (b) HRTEM image.

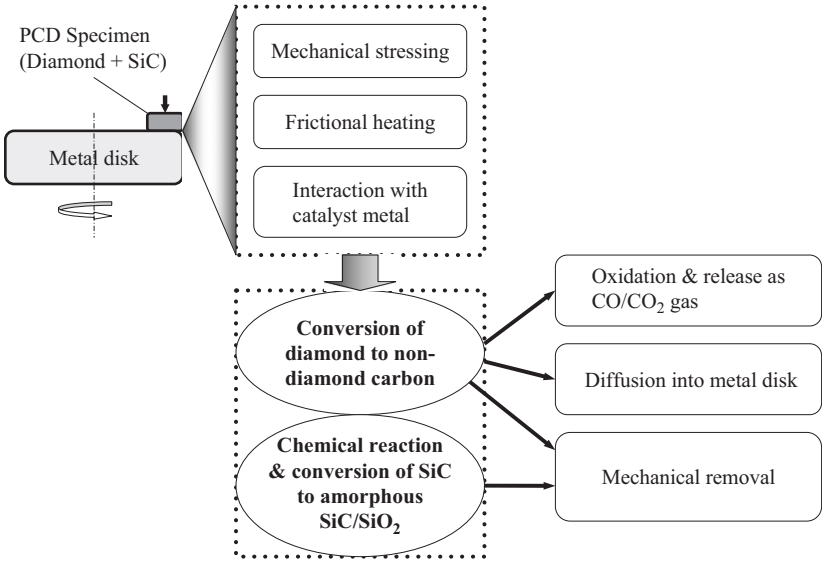

Fig. 8. The mechanism map of material removal in dynamic friction polishing.

4. Conclusions

Based on systematic EELS and HRTEM analyses, it was found that the polishing debris were mainly of amorphous structure, which included different forms of carbon, silicon oxide/carbon, iron oxides, etc. From the free energy theory and low-loss energy spectra, the densities of carbon material in polishing debris were calculated to be much less than diamond. From high-loss energy spectra, the percentage of sp^2 bonding in the hybridized carbon materials of the polishing debris ranged from 30% to 90%. These results indicate that during dynamic friction polishing, the diamond at surface has transformed to amorphous non-diamond carbon due to the interaction with rotating metal disk at elevated temperature. The non-diamond carbon is then mechanically/chemically removed as it is weakly bonded. Additionally, silicon carbide takes part in chemical reactions and transforms to amorphous silicon carbide/oxide. The mechanism map in Fig. 8 provides a guideline for a possible process optimization.

Acknowledgments

The authors wish to thank the Australian Research Council and Ringwood Diamond Material Technologies Pty. Ltd. for their financial support for this research project. The diamond compacts used in the tests were provided by Ringwood. The authors also acknowledge the assistance from the staff, particularly Shaun Bulcock at the Electron Microscope Unit, The University of Sydney.

References

[1] Y. Chen, L.C. Zhang, J.A. Arsecularatne, C. Montross, Polishing of polycrystalline diamond by the technique of dynamic friction, part 1: prediction of the interface temperature rise, International Journal of Machine Tools and Manufacture 46 (6) (2006) 580–587.

[2] K. Suzuki, N. Yasunaga, Y. Seki, A. Ide, N. Watanabe, T. Uematsu, Dynamic friction polishing of diamond utilizing sliding wear by rotating metal disc, Proceedings of ASPE (1996) 482–485.

[3] M. Iwai, T. Uematsu, K. Suzuki, N. Yasunaga, High efficiency polishing of PCD with rotating metal disc, Proceedings of ISAAT2001 (2001) 231–238.

[4] K. Suzuki, M. Iwai, T. Uematsu, N. Yasunaga, Material removal mechanism in dynamic friction polishing of diamond, Key Engineering Materials 238–239 (2003) 235–240.

[5] M. Iwai, Y. Takashima, K. Suzuki, T. Uematsu. Investigation of polishing condition in dynamic friction polishing method for diamond, in: Seventh International Symposium on Advances in Abrasive Technology, Buras, Turkey, 2004.

[6] Y. Chen, L.C. Zhang, J. Arsecularatne, Polishing of polycrystalline diamond by the technique of dynamic friction, part 2: Material removal mechanism,, International Journal of Machine Tools and Manufacture 47 (10) (2007) 1615–1624.

[7] S.E. Grillo, J.E. Field, Investigation of the possibility of electrical wear by sparking in diamond polishing, Wear 211 (1) (1997) 30–34.

[8] H.K. Schmid, Phase identification in carbon and Bn systems by Eels, Microscopy Microanalysis Microstructures 6 (1) (1995) 99–111.

[9] P.J. Fallon, L.M. Brown, Analysis of chemical-vapour-deposited diamond grain boundaries using transmission electron microscopy and parallel electron energy loss spectroscopy in a scanning transmission electron microscope, Diamond and Related Materials 2 (5–7) (1993) 1004–1011.

[10] S. Welz, Y. Gogotsi, M.J. McNallan, Nucleation, growth, and graphitization of diamond nanocrystals during chlorination of carbides, Journal of Applied Physics 93 (7) (2003) 4207–4214.

[11] D.B. Williams, C.B. Carter, Transmission Electron Microscopy: A Textbook for Materials Science—Vol. 4. Spectrometry, Plenum Press, New York, 1996.

[12] S.E. Grillo, J.E. Field, The polishing of diamond, Journal of Physics D: Applied Physics 30 (1997) 202–209.

[13] H.O. Pierson, Handbook of Carbon, Graphite, Diamond and Fullerences: Properties, Processing and Applications, Noyes Publications, New Jersey, USA, 1993.

[14] F.M. van Bouwelen, J.E. Field, L.M. Brown, Electron microscopy analysis of debris produced during diamond polishing, Philosophical Magazine 83 (7) (2003) 839–855.
[15] J. Li, Q. Zhang, S.F. Yoon, J. Ahn, Q. Zhou, S. Wang, D. Yang, Q. Wang, Erosion resistance of polycrystalline diamond films to atomic oxygen, Carbon 41 (9) (2003) 1847–1850.
[16] C.C. Ahn, O.L. Drivanek, R.P. Burgner, M.M. Disko, P.R. Swann, Eels Atlas, A Reference Guide of Electron Energy Loss Spectra Covering all Stable Elements, Gatan Inc., Warrendale, PA, USA, 1983.